Photocurrent generation in artificial light-harvesting protein matrices

Yuval Agam and Nadav Amdursky*

Schulich Faculty of Chemistry, Technion – Israel Institute of Technology, Haifa 3200003, Israel.

*Corresponding author

Dr. Nadav Amdursky,

Schulich Faculty of Chemistry, Technion – Israel Institute of Technology, Haifa, 3200003, Israel

Tel: +972-4-8295953

e-mail: amdursky@technion.ac.il

Keywords

biopolymers, electron transfer, chlorophylls, photocurrent, light-harvesting

Abstract

Global interest in solar energy utilization is driving the search for new materials that allow light harvesting and photocurrent generation under a light stimulus. Light harvesting is also one of the most important natural phenomena, of which photosynthesis is an example, and such natural systems have been as well for photocurrent generation. Inspired by natural light-harvesting complexes, we present here a synthetic and artificial solid-state protein-based biopolymer that facilitates the formation of a photocurrent in a wide range of wavelengths upon the molecular doping of the natural light-harvesting chlorophyll molecules. Interfacing of the doped protein matrix with electrodes yielded a photocurrent in the order of a few microamperes when the matrix was exposed to light. We show a switchable (flipping in the) photocurrent behavior when: 1) the magnitude of the applied bias is changed, 2) the location of the irradiated area is changed with respect to the electrodes, and 3) a gradient doping, enabled by the facile molecular doping approach, is formed. Finally, the synthetic artificial nature of the protein matrix allows the exploration of several light-harvesting cofactors not used in natural systems, where we further show photocurrent generation by doped metal-free porphyrins.

Introduction

Our modern lives and related environmental concerns dictate the growing demand for renewable and non-polluting energy sources, and therefore, considerable effort is being employed to harness natural resources, in particular sunlight, for energy production. Solar energy can be used directly as thermal energy or converted to electricity using photovoltaics materials. Thus, researchers are pursuing new materials that can provide current upon light illumination. Natural light-harvesting complexes, such as the photosystem (PS), drew some attention in this direction because of their natural function in producing energy upon light excitation. Previous studies revealed the possibility of generating photocurrents using the PS protein[1-11] and of utilizing the protein in photovoltaic devices[12,13] and solar cells.[14-17] The use of the PS protein in such devices requires a deposition process of the PS, resulting in a monolayer or a multilayer film, and thus, it has to be formed on a surface, such as an electrode or gold nanoparticle.[1] Furthermore, in most studies the photocurrent generation was achieved in an electrochemical setup, i.e., in an aqueous solution, which can be a limiting factor. In natural systems, the light energy is harvested by a myriad of chromophores situated within proteins, one of the most common ones of which is the chlorophyll (Chl) chromophore. Chl by itself was also tested for its ability to serve as a light-harvesting moiety, where a monolayer or multilayers of Chl were deposited on metal or semiconducting electrodes, resulting in photocurrent generation in a photoelectrochemical setup.[18-23]

Inspired by the natural role of the PS, we designed in this study a synthetic free-standing protein-based polymeric platform that facilitates photocurrent production. The platform is based on electrospun bovine serum albumin (BSA) mats that were molecularly doped with Chl chromophores. The free-standing protein matrix used here has two main advantages. The first is related to the molecular doping approach. It is well known that the BSA protein can bind a myriad of different molecules[24] in a process we refer to as molecular doping. We showed previously that this process can induce long-range electron transport across the doped mat.[25,26] The second advantage is having

a solid-state free-standing biopolymer that contains large (>100 wt.%) water content. Thus, the resultant free-standing mat can be measured in a solid-state two-terminal device configuration, as described in this paper, and at the same time eliminating the need for an electrochemical setup though the photocurrent mechanism is identical to the one in electrochemical cells. At last, the artificial nature of our system, as opposed to natural systems, allows us to modulate its properties easily, and we show the manner in which the gradient doping of the Chl into the mat can change its light responsiveness. The solid-state 2-electrode configuration, together with the possibility of forming gradients of the molecular dopant, results in a simple polarization-dependent photocurrent device. We also show that other chromophores (those that nature does not use for light harvesting) can be molecularly doped into the mat, resulting in similar light responsiveness of the system. All in all, the free-standing protein matrices presented here represent a new family of polymeric materials for light harvesting, and while the purpose of this study is not to target the making of an efficient organic solar cell, the concepts we present here can be utilized for the future integration of polymers in such devices, which are currently dominated by thin layers of organic semiconductors.

Results and Discussion

Our solid-state protein matrix is a resultant of an electrospinning process using only solvated BSA protein. The free-standing material has a fibrillar structure (**Figure S1**) with a thickness of ~70 µm and it can contain a significant amount of water ~100-150 wt.%. The formed mat was then placed in an aqueous solution of Chl, resulting in spontaneous irreversible binding of the Chl molecules to the mat in a process we refer to as molecular doping (**Figure 1a**). As shown previously,[25,26] this straightforward doping strategy results in highly doped protein mats with doping density in the order of $2\text{-}3\times10^{19}$ cm^{-3}. After the successful binding of the Chl molecules to the protein matrix, we investigated the mat's electrical properties. First, we measured the conductivity of the Chl-doped mat using electrochemical impedance spectroscopy (EIS) by laying the mat on gold finger electrodes with a separation distance of 1 mm (**Figure 1b**). By fitting the EIS measurement to an equivalent

circuit (**Figure 1b**, inset), we extracted a bulk conductivity value of 3.1 ± 0.6 mS·cm^{-1} for the Chl-doped mat.

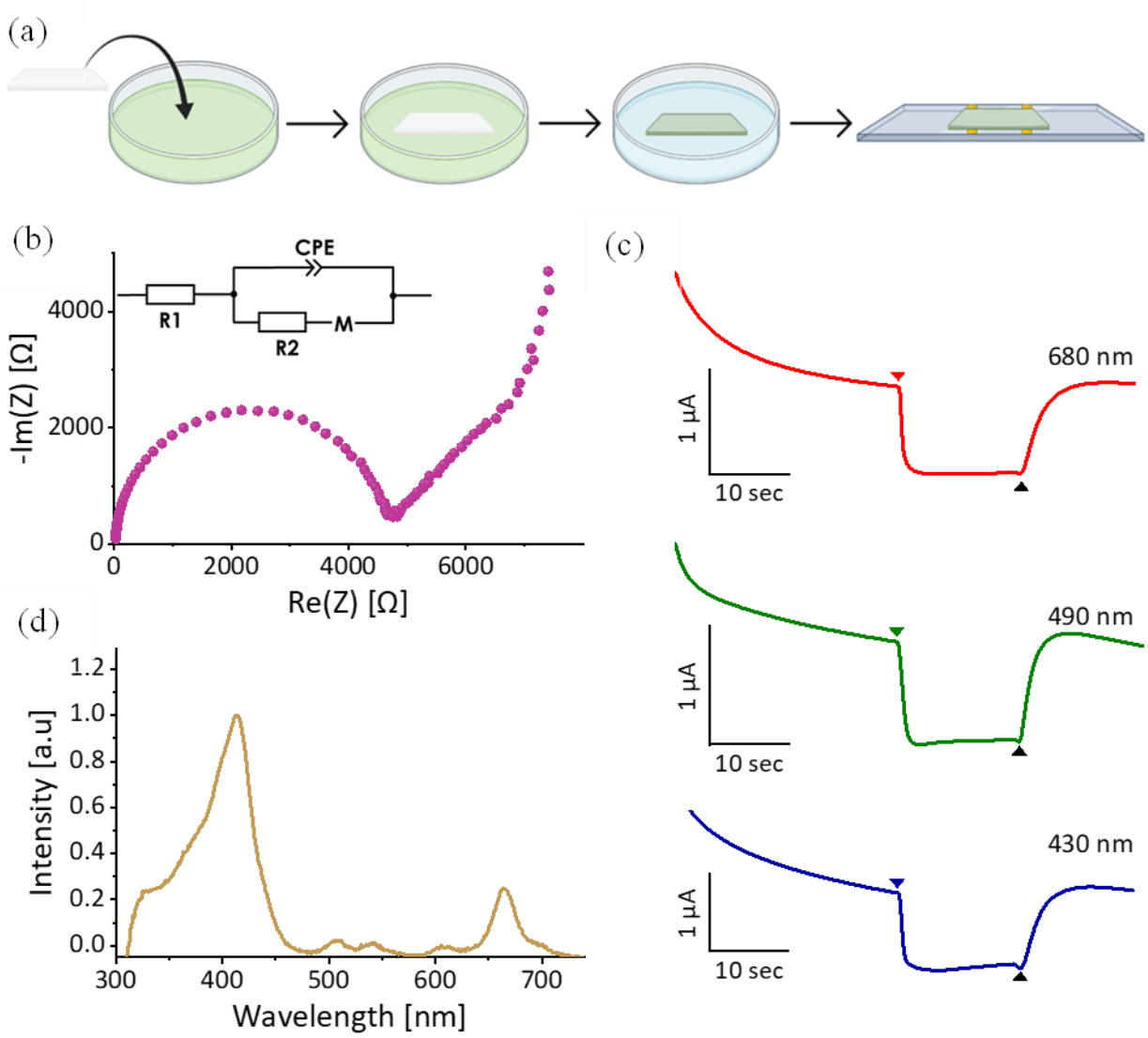

Figure 1. (a) Schematic of the doping process. A BSA mat is placed in a doping solution of Chl, resulting in the binding of the Chl into the protein matrix. (b) Impedance response in the form of a Nyquist plot across a Chl-doped mat with an inter-electrode distance of 1 mm. The inset shows the equivalent circuit used to extract the resistance of the Chl-doped mat. (c) Photocurrent response of the Chl-doped mat with different excitation wavelengths. (d) UV–Vis absorbance spectrum of the used Chl.

For the light harvesting photocurrent generation type of measurements, we used current–time (I–T) measurements upon the application of a DC bias in the same experimental setup as for the EIS measurements, i.e., a terminal device with the mat bridging two gold electrodes. It is important to note that this configuration is symmetric, and it is not a solar cell configuration. During these measurements, we light-irradiated the mat using different wavelengths with the purpose of studying the photocurrent characteristic (**Figure 1c** for a fixed bias of 1.5 V). As shown in the figure, we observed a drop in current under light irradiation. A decrease in conduction upon illumination, also known as negative photoconductivity, was previously observed in semiconductors,[27-29] metal nanoparticles,[30] carbon nanotubes,[31] and even in protein-based materials (incorporated with metal nanoparticles).[32] One main explanation for the negative photoconductivity phenomenon is based on a trapping effect, where impurities can trap the photo-induced carriers, resulting in a decrease in charge density. Such a trapping effect and other suggested mechanisms are expected to change the bulk conductivity across the material upon light irradiation. Importantly, our EIS measurements show identical bulk conductivity of the doped protein matrix under dark conditions and under light illumination (**Figure S2**), and thus, the negative photoresponse in our material cannot be explained by the trapping phenomenon. Instead, as discussed below, all our solid-state measurements indicate the involvement of an anodic photocurrent process taking place next to the two electrodes in the solid state, with some similarities to common electrochemical photocurrent generation, whereas the protein matrix and its trapped water environment is fundamental in the electronic (hole) quenching process of the photocurrent (see discussion below).

Our measured negative photoconductivity, having a current reduction of ~1 μA that can be translated to a reduction in photocurrent density of ~10 $\mu A \cdot cm^{-2}$, is independent of the excitation wavelengths (**Figure 1c**). This finding is very surprising, as the three excitation wavelengths used are in different regions of the UV–Vis absorption of the Chl used in this study (**Figure 1d**), showing fundamental different absorption coefficients for these three different wavelengths: 430 nm in the Soret band,

490 nm in a region with very low absorption, and 680 nm in the Q band region. As shown in the studies having the PS as the light-harvesting molecule,[4,12] the photocurrent magnitude should follow the action spectrum (absorption), meaning that the more photons absorbed, the higher the photocurrent. The fact that we do not see a major change in the photocurrent generation at different wavelengths indicates that our protein matrix is heavily doped, and even when using wavelengths where the doped mat has a low absorption coefficient, we are saturating the photocurrent generation, and that all electronic transitions are resulting in a photocurrent. In an important control experiment, performed with a non-doped BSA mat, we observed a very minor photocurrent only while using the 430 nm blue light (that can be ascribed to a photoelectric effect of the electrodes), and no photocurrent was observed while using a longer wavelength (**Figure S3**). Accordingly, and because of the advantageous use of the long-wavelength low-energy red light, we primarily used it for the rest of the measurements below.

Next, we turned to exploring the role of the applied bias on the photocurrent (**Figure 2a**), showing a flip in the photocurrent direction as a function of the voltage magnitude. Whereas above we described a decrease in photocurrent at a high (1.5 V) bias, the application of lower than 0.8 V biases results in an increase in the photocurrent. We also measured the current while sweeping the voltage (I–V) between 0 V to 1.5 V under light and dark conditions (**Figure S4**), which further supports our observation of flipping in the current direction as a function of applied bias, whereas at low biases, the light current is higher than the dark current, and *vice versa* at higher biases.

The flip in the photocurrent generation can be explained by considering the valence and conduction band alignment with respect to the electrodes. As mentioned above, to date, most of the photocurrent generation studies in which proteins were used involved an electrochemical setup. However, because of our solid-state configuration, it is essential to consider the different processes next to each of the two electrodes. We previously showed that a porphyrin-doped mat has a p-type carrier behavior.[26] The hole transfer (or hole accepting) capabilities of the Chl molecules hint at the involvement of an

anodic photocurrent mechanism rather than a cathodic one. Regardless of the voltage used, the process starts with a photon exciting the Chl and creating an electron–hole pair. At low voltages (**Figure 2b**), the excited electron can flow from the conduction band to the anode and thus increase the current. However, above a critical voltage, which from our experiments we estimate to be around 0.9 V (**Figure 2c**), the anode potential is lower than the valence band of our material. In the latter case, there is no preference for the excited electrons, and thus, no increase in current should occur. On the other hand, considering the process on the other electrode, the excited electrons can be transferred from the conduction band to the cathode, thus decreasing the overall current. In the low voltage regime, the competing process on the anode is favorable because of the potential on the mat, resulting in a slight increase in current.

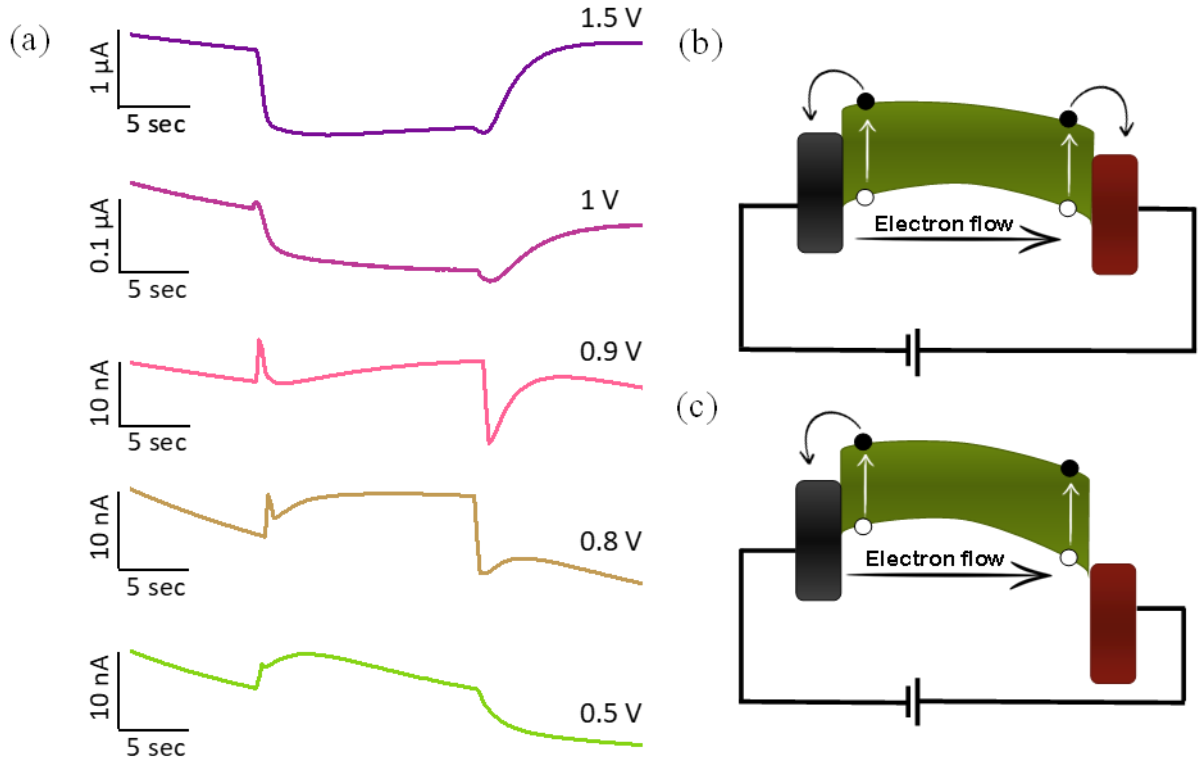

Figure 2. (a) Photocurrent response of the Chl-doped mat under varying DC biases. (b) Suggested photocurrent mechanism under low voltage and (c) high voltage. The red and black shapes represent the anode and cathode potential, respectively.

Whereas photocurrent switching is common and was observed in electrochemical setups,[4,33-36] it is uncommon in solid-state type devices and requires a complex field-effect transistor configuration. In this context, photoconductivity switches from positive to negative were demonstrated by adjusting the wavelength,[37] laser intensity,[38] or gate bias.[39] In our system, the photoconductivity modulation can be achieved by simply changing the external voltage between the source and drain. Since our proposed mechanism involves anodic photocurrent generation (in a similar fashion to an electrochemical setup), a quencher is required to serve as the source for hole recombination. While it is impossible to pinpoint the exact quencher in our protein matrices, the presence of many functional groups of the protein together with a large water content within the protein-based solid-state matrix (up to 150 wt.% of water) can be considered as the source of the quenching process. To have an insight into the role of the protein as the quencher of the process that also allows the reversibility of the process, we have performed two control experiments. The first is to deposit on the electrodes a solution of solvated BSA following the integration of Chl into them. This control experiment has the same 'ingredients' as our main study, but not in a free-standing solid-state biopolymer configuration, thus, it is resembling 'common' photoelectrochemical studies. In this control experiment, we can see a similar drop in current at high biases (Figure S5a) that is in line with the discussed results with the Chl-doped BSA mat (Figure 2a), but the reversibility upon returning to dark was much slower in the solvated protein configuration in comparison to the mat configuration, which can be ascribed to diffusion-limited processes. The second control experiment is to deposit Chl without protein on our device (in an aqueous solution), thus directly targeting the role of the protein in the process. As can be observed in Figure S5b, without the protein, the Chl can also induce the negative photoresponse at higher biases, albeit with a smaller magnitude. However, unlike the experiment with the protein mat or with solvated proteins, using only Chl is resulting in a non-reversible process, meaning that after returning to dark conditions, the current did not go up

again. Accordingly, we can conclude that the protein has a major role in the quenching process of donating a hole and bringing the system to its initial state (before the light excitation).

To confirm our assumptions regarding the photocurrent mechanism, we irradiated each electrode individually (**Figure 3a**), as opposed to irradiating the entire mat uniformly as when the above measurements were taken, while recording the current response at 1.5 V (**Figure 3b**). To do so, we used a longer inter-electrode distance of 8 mm. Whereas placing the illumination beam above the anode resulted in a slight increase in current, the opposite configuration (above the cathode) resulted in a sharp decrease. Moreover, this reduction was more prominent than when the beam was located in the middle of the mat. The vast difference in the photocurrent behavior that can be attributed only to the location of the illumination strongly validates our suggested mechanism. Under high bias, the illumination of the anode does not promote new favored electron pathways (**Figure 3c**). However, irradiation near the cathode allows the excited electrons to flow from the conduction band to the electrode (**Figure 3d**). As we hypothesized, the overall photocurrent in the high voltage regime is dominated solely by processes next to the cathode.

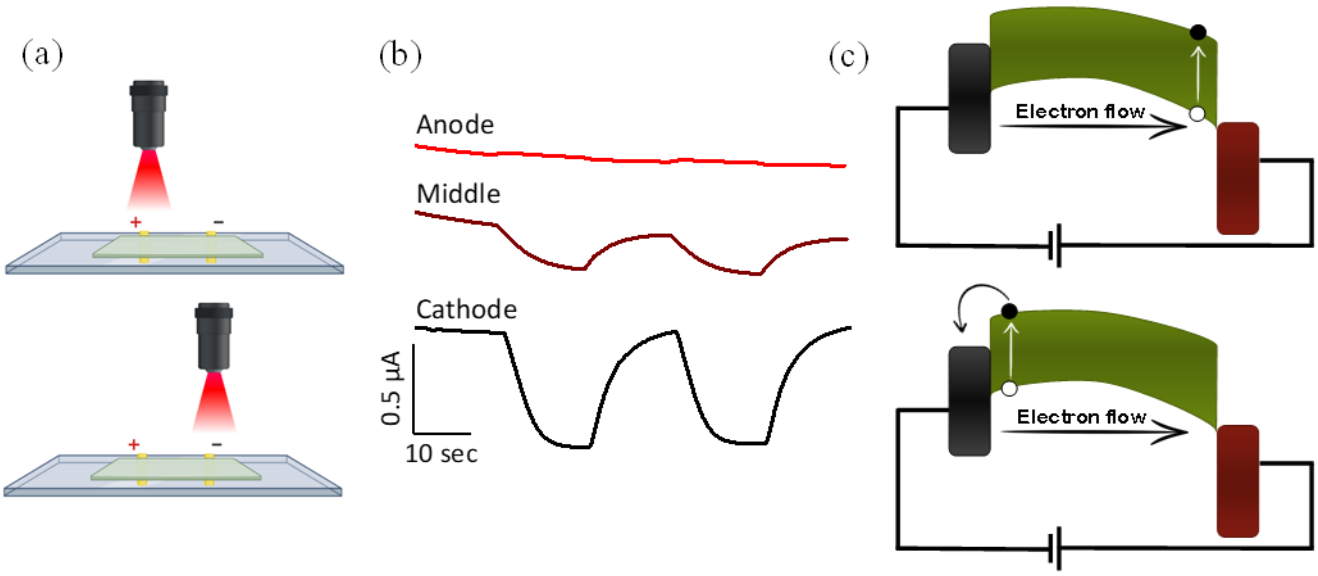

Figure 3. (a) Schematic of the measurement system when irradiation is located above the anode (top) and cathode (bottom). (b) Photocurrent response of the doped mat under a bias of 1.5 V upon illuminating the mat above the anode, in the middle, and above the cathode. (c) Suggested

photocurrent mechanism under 1.5 V bias when the illumination beam is located above the anode (top) and cathode (bottom). The red and black shapes represent the anode and cathode potential, respectively.

Above, we described the modulation of the observed photocurrent generation of our fully doped mat as a function of applied bias and the location of the irradiated area. We now address the use of a gradient-doped mat. As shown in our previous study,[26] the simplicity of our molecular doping method enables easy control of the dopants' concentration. In our study, we utilized this advantage to form a gradient-doped mat, one end of which is fully doped and the second end is non-doped. This approach breaks the symmetry in our system and allows the Chl molecules to interface only with a certain electrode, depending on the configuration. **Figure 4a** shows the position of the gradient-doped mat, where the Chl was next to the anode and an 0-0.3 V voltage was applied. In this setup, the irradiation (of the entire sample) resulted in an increase in the current. However, when we inverted the orientation of the mat with respect to the electrodes, a decrease in current was observed for the same bias regime (**Figure 4b**). We can use a band alignment similar to that described above to explain these results (**Figure 4c**). In zero bias mode, the potential on both electrodes is equal, and therefore, our suggested model predicts that an excited electron will flow from the conduction band to the nearby electrode. When the Chl is located next to the anode, the excitation causes electrons to shift in the current direction. In the opposite case, when the Chl is located next to the cathode, the excited electrons flow in the reverse direction, and hence, the chromophore's location dictates the photocurrent direction.

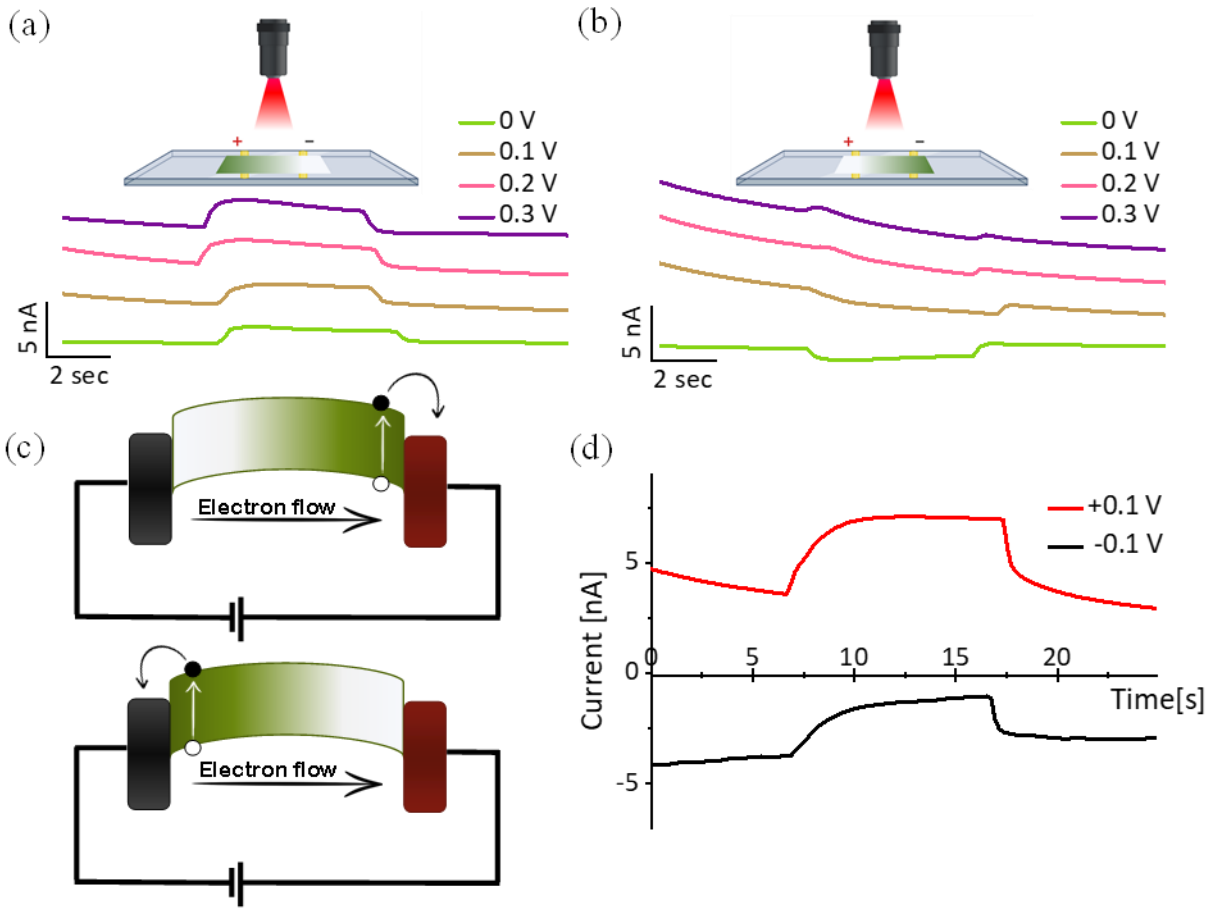

Figure 4. Photocurrent response in the low-voltage regime when the doped part was next to (a) the anode and (b) the cathode. (c) Suggested photocurrent mechanism under zero bias when the Chl dopants are located on the anode (top) and cathode (bottom). The red and black shapes represent the anode and cathode potential, respectively. (d) Photocurrent response when the doped part was next to the anode and the bias polarization was changed.

We further used this symmetry-breaking gradient-doped mat to construct a bias-dependent photocurrent device. As the bias polarization determines the anode and cathode, we anticipated obtaining a similar performance by simply flipping the bias polarization. To examine this idea, we used the same configuration described above with the doped part next to the anode and changed the applied bias from a positive 0.1 V to a negative -0.1 V (**Figure 4d**). As shown in the figure, the two

conditions offer a vital difference in the photocurrent generated: under a positive bias, a rise in current, and under the negative bias, a decrease in current. Hence, unlike the fully doped mat, where a change in voltage direction produces a mirror image of the current (**Figure S6**), when the gradient-doped mat is used, the voltage polarization determines the photocurrent direction.

What distinguishes our system compared to any natural system is the flexibility in choosing the light-harvesting molecule within the protein. Accordingly, in our final section, we show the results of an experiment in which we switched from using Chl as the light-absorbing chromophore to using protoporphyrin IX (PPIX) as the dopant. As when Chl was used, we observed a significant negative photocurrent upon light excitation at high biases and a switch in the photocurrent polarity when the low-voltage regime was reached (**Figure 5a**). The only difference in the PPIX-doped mat from the Chl-doped one is the observed bias of the photocurrent polarity switching, where in the Chl-doped mat it was around 0.9 V (**Figure 2a**) and in the PPIX-doped mat around 0.5 V. The difference in the switching bias is indicative of the different positions of the valence band between Chl and PPIX (as explained for **Figure 2b**). We further confirmed the recurrence of the negative photocurrent phenomenon by applying a constant voltage of 1 V while repeatedly turning the light on and off in cycles (**Figure 5b**). We also conducted the same experiment again, except that initially the light was switched on, which showed the same trend, i.e., an increase in current when the light is switched off (**Figure S7**). Finally, we also demonstrated that the light intensity can be used as a gating source for controlling the generated photocurrent (**Figure 5c**), whereas the higher the light intensity, the larger the photocurrent response.

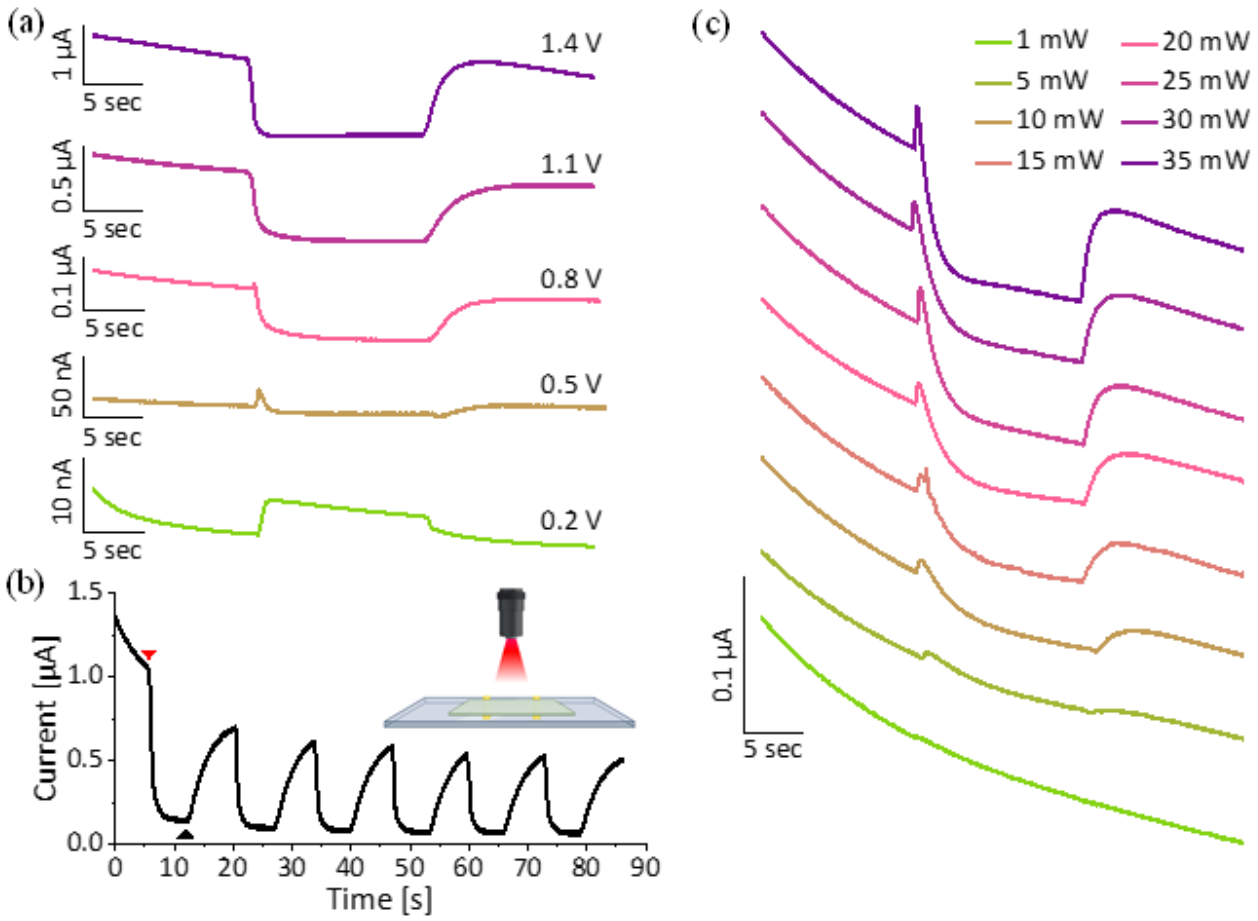

Figure 5. (a) Photocurrent response of the PPIX-doped mat under varying DC biases, and (b) upon cycles of irradiation at a constant 1 V bias. (c) Photocurrent response as a function of the light intensity power.

Conclusions

In summary, we have shown in this paper the manner in which widely available proteins (BSA) can be used for the easy formation of a light-harvesting material capable of supporting photocurrent generation in a solid-state device. While our approach is inspired by the natural role of chromophores in light harvesting within biological systems, our artificial protein material and the straightforward molecular doping methodology eliminate the need for expensive and cumbersome procedures for obtaining purified photosystems. A freestanding macroscopic material also provides an advantage

over natural systems, where the light-harvesting protein is transmembrane. Because of the abundance of our starting material and the simple methodology, our final materials are extremely low cost and can be created on a large scale, and thus, their production can easily be upscaled to a large amount. Furthermore, because of the artificial nature of our systems, we can easily tune the concentration, location, and chemical nature of the light-harvesting molecule, which cannot be achieved using natural systems. The simplicity, tunability, and low cost of our materials, together with the solid-state configuration of our devices, as opposed to the electrochemical setup in common bio-related photocurrent generation devices, is a significant advantage of our approach. While we did not target here the formation of a solar cell, the presentation of a new artificial biomaterial with such modular properties together with the simplicity in its formation can serve as an excellent test bed for any future integration of polymers in light-harvesting applications.

Materials and Methods

Electrospinning of BSA mats: An electrospinning solution was prepared by dissolving BSA (MP Biomedicals) in 90% 2,2,2-trifluoroethanol (Apollo Scientific) for a final BSA concentration of 14% (w/v). After 12 h, 5% (v/v) β-mercaptoethanol (Alfa Aesar) was added. Electrospinning was performed in a custom-built system with a grounded collector. A 15 k V bias was applied on a 24-gauge blunt needle with an injection rate of 1.5 ml/h. The needle was fixed 12 cm above the collector. The final mat thickness was 60 μm.

Doping process: Stock solutions were prepared by dissolving Protoporphyrin IX (STREM chemicals) and chlorophyll (Spectrum, a mixture of chlorophyll a and b) in 1 mL dimethyl sulfoxide (DMSO) (Carlo-Erba) for a final concentration of 3.2 mM. These stock solutions were then diluted with 1 ml DMSO and 5 mL physiological buffered saline (PBS) buffer to yield doping solutions

having a concentration of 0.1 mM. The mats were then placed in the doping solutions on a stirring plate without light exposure for around 24 h.

UV-Vis absorption: UV-Vis absorption of chlorophyll in DMSO was measured with an Agilent Cary 60 spectrophotometer using a quartz cuvette having a 1 cm path length.

Metal finger electrode fabrication: Glass microscope slides were used as substrates for the electrodes. The glass substrates were washed with distilled water and dried using hot air. Using an E-beam evaporator at a deposition rate of 2 $Å s^{-1}$ under 5×10^{-7} Torr at room temperature, 100 nm Au on 10 nm Cr were evaporated through shadow masks. Mats were placed on finger electrodes and gently dried with filter paper to remove excess water.

Impedance measurements: Impedance measurements were performed using an MTZ-35 impedance/gain-phase analyzer (Bio-Logic). Mats were placed on finger electrodes with an inter-electrode distance of 1 mm and the electrodes were contacted using a probe station micromanipulator. A 50 mV AC bias was applied during the measurements without DC bias. A frequency range of 10 MHz to 10 Hz was used.

I-T measurements: Current–time measurements were conducted using B2901A (Keysight Technologies). The desired voltage was applied, and the current was recorded against time. We set a light emitting diode (with wavelengths of 680 nm, 490 nm, or 405 nm) above the mat and turned the light on and off at specified intervals. The irradiation power was controlled by the power controller and determined using a power meter. Gold finger electrodes distanced at 1 mm or 8 mm were used for the current–time measurements.

Supporting Information

Supporting Figures (Figure S1-S7) can be found online.

Acknowledgments

Y.A. thanks the Jacobs Fellowship for financial support. N.A. thanks the Ministry of Science and Technology (Nos. 3-16243, 3-16312, and 3-17367). We thank the Grand Technion Energy Program (GTEP) and the Russel Berrie Nanotechnology Institute (RBNI) for their support in equipment use.

Declaration of Interests

The authors declare no competing interests.

References

(1) Terasaki, N.; Yamamoto, N.; Hiraga, T.; Sato, I.; Inoue, Y.; Yamada, S. *Thin Solid Films* **2006**, *499*, 153.

(2) Carmeli, I.; Frolov, L.; Carmeli, C.; Richter, S. *J. Am. Chem. Soc.* **2007**, *129*, 12352.

(3) Ciesielski, P. N.; Scott, A. M.; Faulkner, C. J.; Berron, B. J.; Cliffel, D. E.; Jennings, G. K. *ACS Nano* **2008**, *2*, 2465.

(4) Ciesielski, P. N.; Faulkner, C. J.; Irwin, M. T.; Gregory, J. M.; Tolk, N. H.; Cliffel, D. E.; Jennings, G. K. *Adv. Funct. Mater.* **2010**, *20*, 4048.

(5) Wolfe, K. D.; Gargye, A.; Mwambutsa, F.; Than, L.; Cliffel, D. E.; Jennings, G. K. *Langmuir* **2021**, *37*, 10481.

(6) Faulkner, C. J.; Lees, S.; Ciesielski, P. N.; Cliffel, D. E.; Jennings, G. K. *Langmuir* **2008**, *24*, 8409.

(7) Manocchi, A. K.; Baker, D. R.; Pendley, S. S.; Nguyen, K.; Hurley, M. M.; Bruce, B. D.; Sumner, J. J.; Lundgren, C. A. *Langmuir* **2013**, *29*, 2412.

(8) Wang, P.; Frank, A.; Zhao, F.; Szczesny, J.; Junqueira, J. R. C.; Zacarias, S.; Ruff, A.; Nowaczyk, M. M.; Pereira, I. A. C.; Rögner, M.; Conzuelo, F.; Schuhmann, W. *Angew. Chem. Int. Ed.* **2021**, *60*, 2000.

(9) LeBlanc, G.; Chen, G.; Gizzie, E. A.; Jennings, G. K.; Cliffel, D. E. *Adv. Mater.* **2012**, *24*, 5959.

(10) Heifler, O.; Carmeli, C.; Carmeli, I. *J. Phys. Chem. C* **2018**, *122*, 11550.

(11) Frolov, L.; Rosenwaks, Y.; Carmeli, C.; Carmeli, I. *Adv. Mater.* **2005**, *17*, 2434.

(12) Das, R.; Kiley, P. J.; Segal, M.; Norville, J.; Yu, A. A.; Wang, L.; Trammell, S. A.; Reddick, L. E.; Kumar, R.; Stellacci, F.; Lebedev, N.; Schnur, J.; Bruce, B. D.; Zhang, S.; Baldo, M. *Nano Lett.* **2004**, *4*, 1079.

(13) Frolov, L.; Rosenwaks, Y.; Richter, S.; Carmeli, C.; Carmeli, I. *J. Phys. Chem. C* **2008**, *112*, 13426.

(14) Gizzie, E. A.; Scott Niezgoda, J.; Robinson, M. T.; Harris, A. G.; Kane Jennings, G.; Rosenthal, S. J.; Cliffel, D. E. *Energy Environ. Sci.* **2015**, *8*, 3572.

(15) Gordiichuk, P. I.; Wetzelaer, G.-J. A. H.; Rimmerman, D.; Gruszka, A.; de Vries, J. W.; Saller, M.; Gautier, D. A.; Catarci, S.; Pesce, D.; Richter, S.; Blom, P. W. M.; Herrmann, A. *Adv. Mater.* **2014**, *26*, 4863.

(16) Mershin, A.; Matsumoto, K.; Kaiser, L.; Yu, D.; Vaughn, M.; Nazeeruddin, M. K.; Bruce, B. D.; Graetzel, M.; Zhang, S. *Scientific Reports* **2012**, *2*, 234.

(17) Torabi, N.; Rousseva, S.; Chen, Q.; Ashrafi, A.; Kermanpur, A.; Chiechi, R. C. *RSC advances* **2022**, *12*, 8783.

(18) Tang, C. W.; Albrecht, A. C. *J. Chem. Phys.* **1975**, *62*, 2139.

(19) Boussaad, S.; Hotchandani, S.; Leblanc, R. M. *Appl. Phys. Lett.* **1993**, *63*, 1768.

(20) Furukawa, H.; Inoue, N.; Watanabe, T.; Kuroda, K. *Langmuir* **2005**, *21*, 3992.

(21) Miyasaka, T.; Honda, K. *Surf. Sci.* **1980**, *101*, 541.

(22) Miyasaka, T.; Watanabe, T.; Fujishima, A.; Honda, K. *J. Am. Chem. Soc.* **1978**, *100*, 6657.

(23) Kay, A.; Graetzel, M. *J. Phys. Chem. A* **1993**, *97*, 6272.

(24) Varshney, A.; Sen, P.; Ahmad, E.; Rehan, M.; Subbarao, N.; Khan, R. H. *Chirality* **2010**, *22*, 77.

(25) Amdursky, N.; Wang, X.; Meredith, P.; Riley, D. J.; Payne, D. J.; Bradley, D. D. C.; Stevens, M. M. *Adv. Mater.* **2017**, *29*, 1700810.

(26) Agam, Y.; Nandi, R.; Kaushansky, A.; Peskin, U.; Amdursky, N. *Proc. Natl. Acad. Sci. U.S.A* **2020**, *117*, 32260.

(27) Wei, P.-C.; Chattopadhyay, S.; Yang, M.-D.; Tong, S.-C.; Shen, J.-L.; Lu, C.-Y.; Shih, H.-C.; Chen, L.-C.; Chen, K.-H. *Phys. Rev. B* **2010**, *81*, 045306.

(28) Chang, M. C. P.; Penchina, C. M.; Moore, J. S. *Phys. Rev. B* **1971**, *4*, 1229.

(29) Han, Y.; Zheng, X.; Fu, M.; Pan, D.; Li, X.; Guo, Y.; Zhao, J.; Chen, Q. *Phys. Chem. Chem. Phys.* **2016**, *18*, 818.

(30) Nakanishi, H.; Bishop, K. J. M.; Kowalczyk, B.; Nitzan, A.; Weiss, E. A.; Tretiakov, K. V.; Apodaca, M. M.; Klajn, R.; Stoddart, J. F.; Grzybowski, B. A. *Nature* **2009**, *460*, 371.

(31) Biswas, C.; Jeong, H.; Jeong, M. S.; Yu, W. J.; Pribat, D.; Lee, Y. H. *Adv. Funct. Mater.* **2013**, *23*, 3653.

(32) Gogurla, N.; Sinha, A. K.; Naskar, D.; Kundu, S. C.; Ray, S. K. *Nanoscale* **2016**, *8*, 7695.

(33) Yasutomi, S.; Morita, T.; Imanishi, Y.; Kimura, S. *Science* **2004**, *304*, 1944.

(34) Yasutomi, S.; Morita, T.; Kimura, S. *J. Am. Chem. Soc.* **2005**, *127*, 14564.

(35) Gill, R.; Patolsky, F.; Katz, E.; Willner, I. *Angew. Chem. Int. Ed.* **2005**, *44*, 4554.

(36) Uji, H.; Tanaka, K.; Kimura, S. *J. Phys. Chem. C* **2016**, *120*, 3684.

(37) Jawa, H.; Ghosh, S.; Varghese, A.; Sahoo, S.; Lodha, S. *arXiv preprint arXiv:2111.00766* **2021**.

(38) Kim, H. J.; Lee, K. J.; Park, J.; Shin, G. H.; Park, H.; Yu, K.; Choi, S.-Y. *ACS Appl. Mater. Interfaces* **2020**, *12*, 38563.

(39) Wang, Y.; Liu, E.; Gao, A.; Cao, T.; Long, M.; Pan, C.; Zhang, L.; Zeng, J.; Wang, C.; Hu, W.; Liang, S.-J.; Miao, F. *ACS Nano* **2018**, *12*, 9513.

Supporting information

Photocurrent generation in artificial light-harvesting protein matrices

Yuval Agam and Nadav Amdursky*

Schulich Faculty of Chemistry, Technion – Israel Institute of Technology, Haifa 3200003, Israel.

*Corresponding author e-mail: amdursky@technion.ac.il

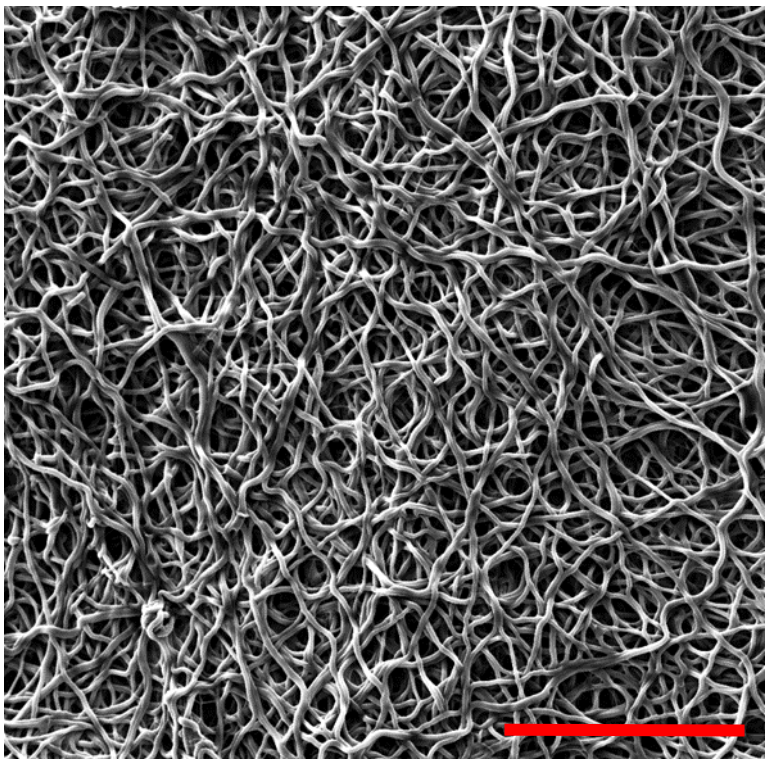

Figure S1. SEM images of the mat, the scale represents 50 μm.

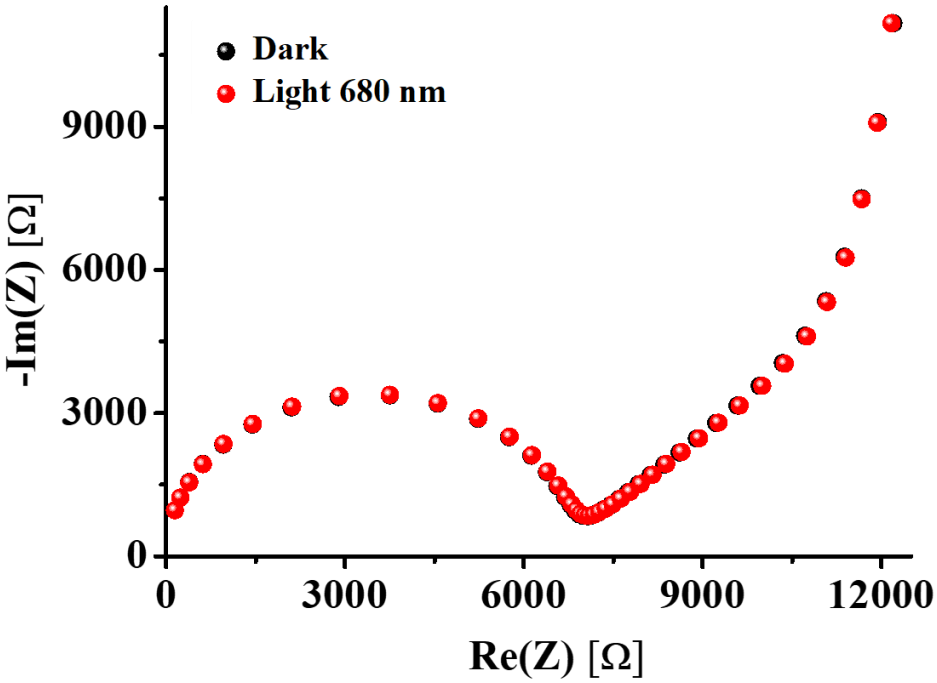

Figure S2. Impedance response in the form of a Nyquist plot across a Chl-doped mat with an inter-electrode distance of 1 mm in the dark and under light irradiation of 680 nm.

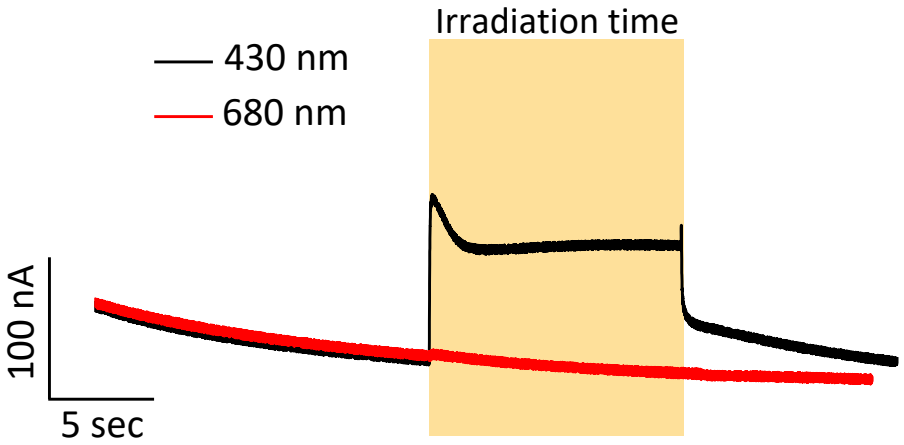

Figure S3. Photocurrent response of the non-doped mat with different excitation wavelengths.

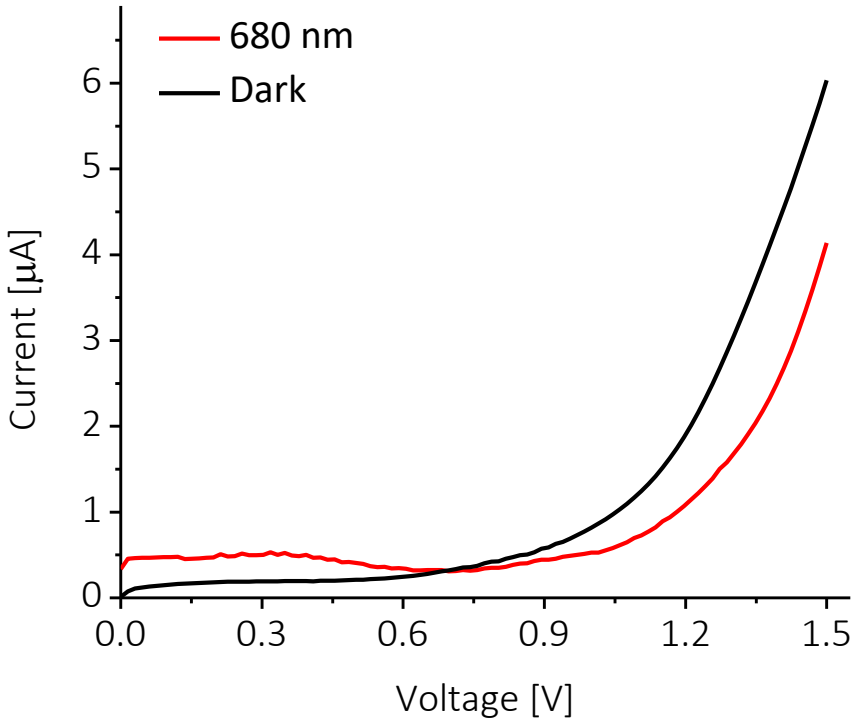

Figure S4. I–V plots of Chl-doped mat in dark and under light irradiation of 680 nm.

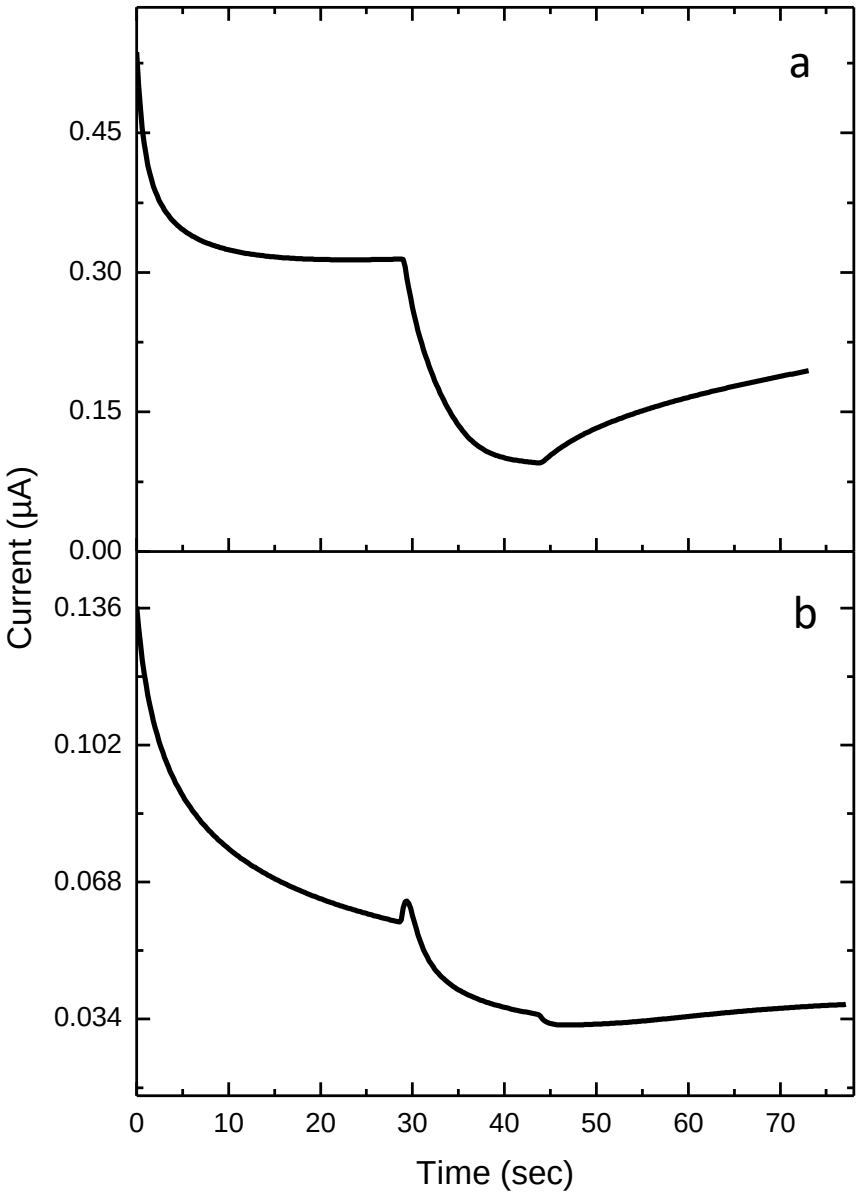

Figure S5. Photocurrent response under 1V bias of the (a) BSA-Chl solution (b) Chl solution.

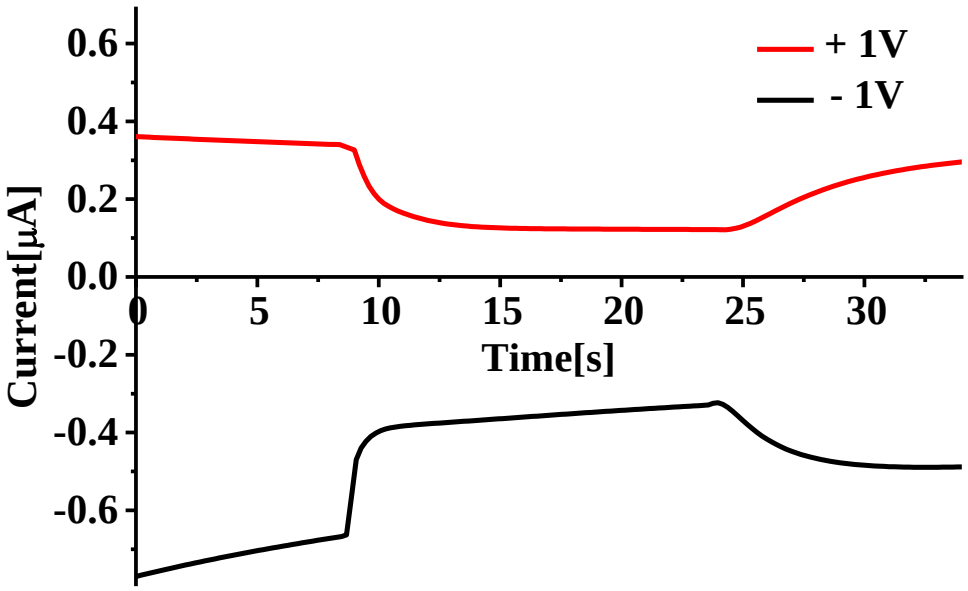

Figure S6. Photocurrent response of the fully Chl-doped mat upon changing the bias polarization.

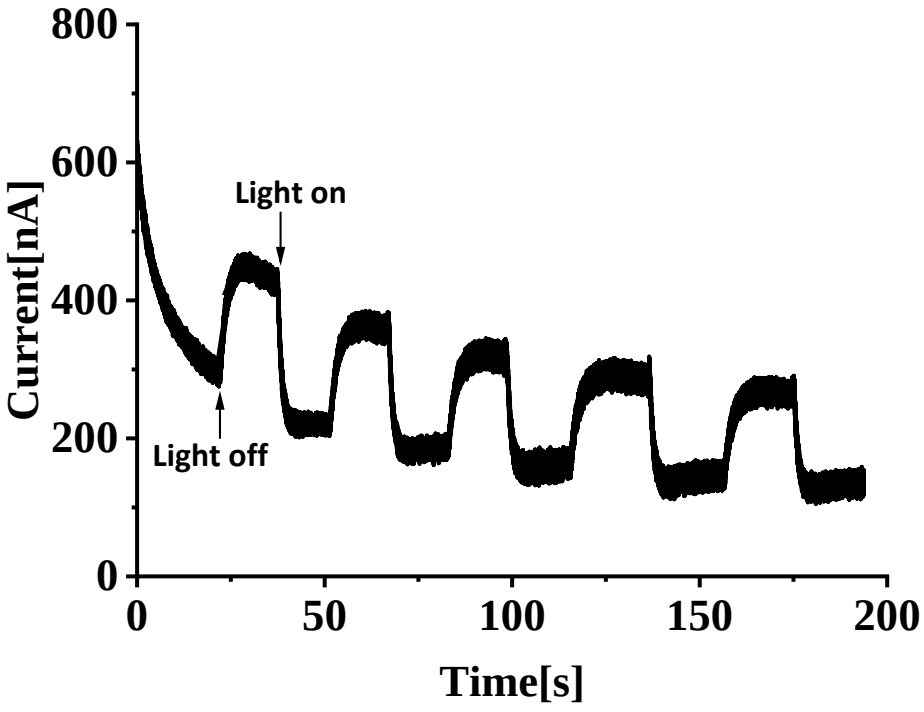

Figure S7. PPIX-doped mat photocurrent cycles under 1V bias.